Topographic anisotropy in continuous magnetic films with two-dimensional surface nanomodulation

S. P. Li, Jeffrey F. Godsell, and Saibal Roy

Citation: Journal of Applied Physics **108**, 093915 (2010); doi: 10.1063/1.3501111
View online: http://dx.doi.org/10.1063/1.3501111
View Table of Contents: http://aip.scitation.org/toc/jap/108/9
Published by the American Institute of Physics

Topographic anisotropy in continuous magnetic films with two-dimensional surface nanomodulation

S. P. Li, Jeffrey F. Godsell, and Saibal Roy[a)]
Tyndall National Institute, University College Cork, Lee Maltings, Cork, Ireland

(Received 18 August 2010; accepted 13 September 2010; published online 5 November 2010)

Artificial and local control of spin-configuration in nanoscale in continuous magnetic films could enable new spin-based electronics and precision sensor technologies. Extensive theoretical research has recently been devoted to examination of surface nanovariation mediated magnetism and its utility, which has been demonstrated only in one-dimensional surface modulation. However, a realization of engineered spin configuration using two-dimensional (2D) nanomodulation is limited by local vortex formation induced by magnetostatic energy. In this work we demonstrate for the first time, an ability to control the anisotropy in continuous magnetic films by periodic surface nanomodulation in two-dimensions (2D). Magnetic properties of NiFe films with nanomodulated surfaces have been studied as a function of both film thickness and modulation amplitude. For films with a patterned square array (without breaking the film continuity), a clear fourfold symmetry of anisotropy field and coercivity was observed with rotation angle. An experimental phase diagram of anisotropy with respect to film thickness and modulation amplitude has been produced which delineates that the observed fourfold anisotropy is induced by the magnetostatic effect. The observed dependence of anisotropy field on film thickness and surface modulation amplitude agrees well with the developed theory. © *2010 American Institute of Physics*. [doi:10.1063/1.3501111]

I. INTRODUCTION

While patterned isolated magnetic structures have been extensively studied,[1–3] structured continuous magnetic films have also drawn considerable attention in recent years.[4–8] Such films could find potential applications in high density information storage and many other spintronic devices.[4–6] Several methods have been used to control magnetization configuration in magnetic films without breaking the film continuity, such as ion irradiation through mask,[4] selective epitaxy,[5] surface modulation,[6–8] etc. Surface nanomodulation is attractive because it provides potentially a low cost, simple method to engineer spin configuration locally in magnetic films, which is essential for many magnetic devices, such as high precision bidimensional magnetic sensors, magnetoresistive devices,[8,9] etc. Magnetic anisotropy induced by surface modulation in one dimension (arrays of lines) has previously been demonstrated.[6–9] On the contrary, to realize a controlled anisotropy in a film by two-dimensional (2D) surface nanomodulation a strict optimization of surface-modulation (both frequency and amplitude), film thickness, intrinsic anisotropy, coercivity, etc. are needed. Strong 2D surface modulation induced magnetostatic energy may force the spins into local vortices, while for a weak surface modulation the intrinsic anisotropy of the magnetic films will dominate the film's properties. Theoretical research on the 2D periodic surface modulation of magnetic films started 40 years ago.[10] Recently, recording and magnetoelectric applications have attracted a great deal of renewed interest in how surface variation/roughening will affect the properties of magnetic films.[11–16] To verify the extensive theoretical works, experiments on magnetic films with well defined, quantified, and specifically designed structures are required. In this manuscript, we present the results of a detailed study into the magnetic behavior of a soft magnetic $Ni_{45}Fe_{55}$ alloy film with a circular nanodent array as surface modulation. We report the experimental verification of tailoring such magnetic properties as, anisotropy, coercivity, etc. through the manipulation of 2D surface topography.

II. EXPERIMENT

A 700 nm thick polymethylmethacrylate (PMMA) film was spun onto a silicon substrate. A nanohole array with 400/400 nm diameter/separation, and 240 nm depth was created by nanoimprinting using an Si stamp. In order to obtain a nanomodulation pattern of varying amplitudes, the hole structure in PMMA was partially planarized by spin coating polystyrene solution in toluene with various concentrations. After 60 min baking at 80 °C, a 10 nm Ti adhesion layer and 200 nm of Au were deposited by sputtering. Four groups of substrates with surface modulation amplitudes (the depth of dent) of 40 nm, 100 nm, 140 nm, and 220 nm, respectively, were prepared. In order to obtain a conformal magnetic film deposition, electroplating was used to deposit the $Ni_{45}Fe_{55}$ magnetic films. During the plating a magnetic field was applied in ⟨10⟩ direction of the square pattern array to introduce uniaxial anisotropy (we refer it as induced anisotropy) in the magnetic films. Magnetic properties were measured using a hysteresis loop tracer (SHB instruments Inc., USA) designed for measurement on ultrasoft magnetic materials (field accuracy 0.01 Oe), where the anisotropy field was defined by a field that correspond to saturation magnetization on initial permeability line. While, coercivity and remanent magneti-

a)Electronic mail: saibal.roy@tyndall.ie.

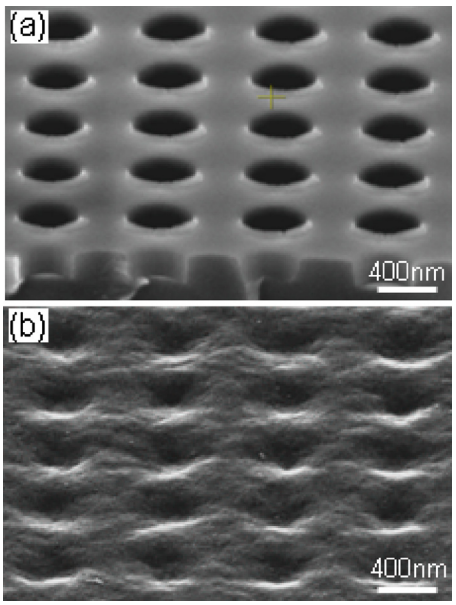

FIG. 1. (Color online) SEM images of the array of nanoholes in PMMA (a) and plated $Ni_{45}Fe_{55}$ film with modulated surfaces (b).

zation were determined by zero-magnetization field and zero-field magnetization on hysteresis loops, respectively.

III. RESULTS AND DISCUSSION

Figure 1(a) and 1(b) show a scanning electron micrograph of an imprinted PMMA structure and a finished sample. Figure 2 displays two typical hysteresis loops [Figs. 2(a) and 2(b)] and a data set [Fig. 2(c)] showing normalized remanent magnetization as a function of the angle between applied field and the film's induced easy axis. These are measured on a sample with 80 nm film thickness and 220 nm

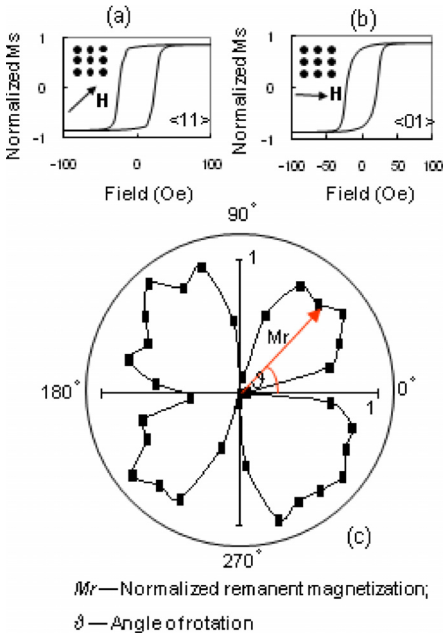

FIG. 2. (Color online) Two typical types of hysterisis loops measured from a ⟨11⟩ (a) and ⟨01⟩ (b) orientations and angle dependence of normalized remanent magnetization of hysterisis loop (c) measured from an 80 nm thick film with 220 nm modulation amplitude.

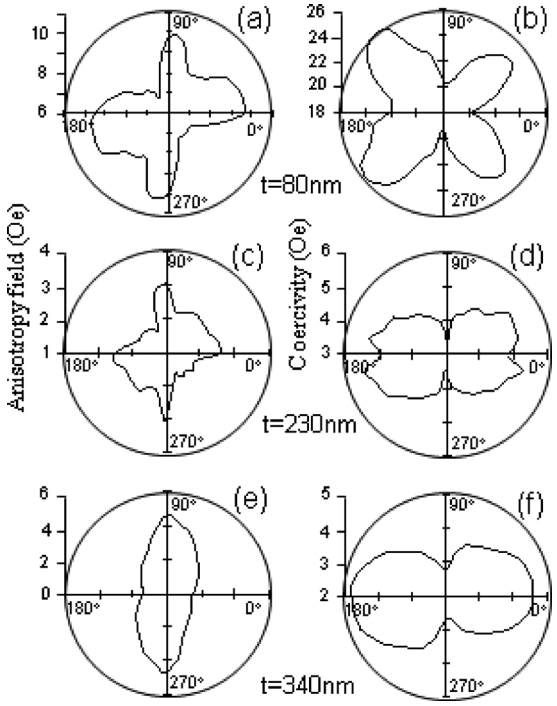

FIG. 3. Angle dependence of anisotropy field (left column) and coercivity (right column) taken from films with 220 nm modulation amplitude and different thicknesses as indicated.

modulation amplitude. To amplify the scale contrast, the remanent magnetization is normalized using a maximum value obtained from a ⟨11⟩ direction and a minimum value from a ⟨01⟩ direction. The hysteresis loops shown in Figs. 2(a) and 2(b) were normalized with magnetization at 1000 Oe where the samples were fully saturated. The most striking feature of the remanent magnetization plot is its fourfold symmetry with abrupt minima in four equivalent ⟨01⟩ directions and four maxima in ⟨11⟩ directions. This suggests that two easy axes were generated in the diagonal ⟨11⟩ directions in the patterned film which are clearly identified by the two types of hysteresis loops in Figs. 2(a) and 2(b). Apparently this signifies the minimization of magnetostatic energy induced by nanomodulation in the two equivalent ⟨11⟩ directions. Although the modulation amplitude is considerably strong, the magnetostatic energy was not able to force the magnetization into local vortices, instead a large remanent magnetization is retained [Fig. 2(b)], which is further explained later. A curious feature of Fig. 2(c) is two satellite maxima besides each main maximum in the ⟨11⟩ directions, which presumably are induced by higher order symmetries of anisotropy as discussed later in the paper. In Fig. 3 we plot measured anisotropy field (H_K) and coercivity (H_C) against rotation angle for films with 220 nm modulation amplitude and film thickness of 80 nm, 230 nm, and 340 nm, respectively. Again, fourfold symmetry of H_K, H_C curves can clearly be seen from the sample with 80 nm film thickness [Figs. 3(a) and 3(b)]. Here the anisotropy fields of a magnetic film, H_K, and coercivity, H_C, are determined from hysteresis loops for each rotation angle. As expected one can see a clear competition between the fourfold anisotropy caused by modulation and the film's twofold induced-anisotropy in the

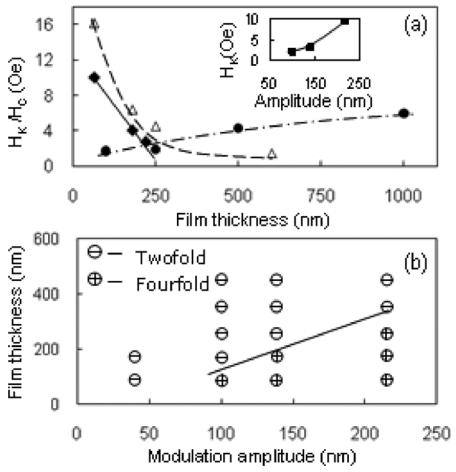

FIG. 4. (a) Thickness dependence of anisotropy field taken from both patterned (diamond), unpatterned films (solid circle), and together with coercivities measured from unpatterned films (open triangle). The anisotropy fields of unpatterned films were taken from hard axes. Inset shows a modulation amplitude dependence of topographic anisotropy. (b) An experimental phase diagram which defines a transition from fourfold topographic anisotropy to twofold induced anisotropy with increasing film thickness and reducing surface modulation.

results measured from the 230 nm thick film [Figs. 3(c) and 3(d)]. The topographic/induced anisotropy falls/rises with increasing film thickness while the relative strength of the anisotropy field at 90° and 270° (induced hard axis) increases and the anisotropy field at 0° and 180° (induced easy axis) decreases. The coercivity drop in the ⟨01⟩ directions can still be seen in this sample [Fig. 3(d)]. By further increasing of the film thickness to more than around 300 nm, the fourfold topographic anisotropy is completely masked by induced anisotropy as shown in Figs. 3(e) and 3(f). The competition between topographic anisotropy and induced anisotropy can be seen more clearly in Fig. 4(a). Here we plot the thickness dependence of the anisotropy fields of the patterned films (220 nm modulation amplitude) as topographic anisotropy values measured on the [10] direction, where the effect of induced anisotropy is minimized. For comparison, a thickness dependence of the induced anisotropy field taken from a batch of unpatterned films is also plotted. For the patterned film we see a nearly linear drop in the anisotropy field with increasing film thickness until eventually the film's induced anisotropy becomes dominant. This drop of topographic anisotropy with increasing film thickness measured in different samples follows a power law $H_k \sim 1/t^{1.25}$. On the other hand the relation between the surface modulation amplitudes "a" and topographic anisotropy fields "H_K" measured in the [10] direction for 80 nm thick films deposited on substrates with different modulation amplitudes is found to follow a power law of $H_K \sim a^{1.7}$ [inset of Fig. 4(a)]. The errors of exponents in the fitted power laws are ±0.1 and ±0.2 for thickness and amplitude dependence, respectively. In combination, these agree closely with the recently developed theory for a magnetic film with both top and bottom surface variation in-phase (vary with the same amplitude in the same direction), $H_K \sim NM_S \sim a^2/t$, where N is demagnetizing factor, t is film thickness, and a is the surface modulation amplitude.[17] As the power law was derived analytically from magnetostatic

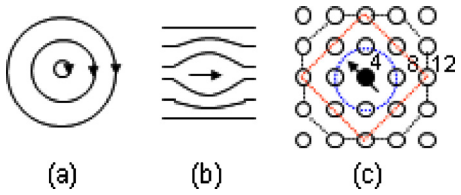

FIG. 5. (Color online) Schematic illustrations of magnetization configurations for vortex (a) and near-single-domain state (b), and how the anisotropy symmetries are contributed by neighbor elements (c). The magnetization configurations in (a) and (b) are illustrated in the vicinity of one nanodent. The numbers 4, 8, and 12 in (c) indicate the folds of symmetry contributed from equivalent numbers of structure elements.

phenomenon (i.e., definition of tensorial demagnetizing factor $\boldsymbol{N}$ using self energy $W=(1/2)4\pi Ad\boldsymbol{M}\cdot\boldsymbol{N}\cdot\boldsymbol{M}$, where A, d, $\boldsymbol{M}$ are a reference area, film thickness, and magnetization, respectively),[10,17] this agreement reveals that the fourfold anisotropy is indeed originated from magnetostatic energy induced by surface modulation. A thickness dependence of film intrinsic coercivity is also shown in Fig. 4(a) to indicate that the surface variation does not much increase film coercivity value, and this offers another advantage of such structured film. Additionally by examination of the variation in peaks in anisotropy fields (H_K) with film thicknesses (t) and modulation amplitudes (a), as typically shown for a particular modulation amplitude in Fig. 3, we are able to plot a phase diagram at various film thicknesses and amplitudes of surface modulation [Fig. 4(b)], and we show a boundary bellow which a fourfold symmetry is maintained.

In the patterned thin films we investigated here, magnetization configurations would be mainly governed by magnetostatic and exchange energy. For a square array-patterned (400 nm dent diameter and 400 nm separation) film with 100 nm thickness and 100 nm modulation amplitude the energy densities we have calculated are 0.49×10^4 and 1.33×10^4 J/m^3 for vortex and near single domain state. The micromagnetic calculation was carried out on 5×5 μm^2 square film with 5×5 nanodent array using OOMMF code.[18] The additional magnetostatic energy created on the edge of the film was calibrated by a calculated magnetostatic energy from a 5×5 μm^2 blank film with the same thickness and material parameters, which are, film thickness: 100 nm, cell size: 20 nm, anisotropy constant: $K_1=600$ J/m^3, exchange constant: $A=6.47\times10^{-12}$ J/m, saturation magnetization: $M_S=1.2\times10^6$ A/m.

The calculated result shows that the energy of vortex state [Fig. 5(a)] is comparable to that of a near-single-domain remanent state [Fig. 5(b)] and even lower. This indicates that there is strong intention to adopt vortex state in the 2D nanomodulated films. The experimentally obtained near-single-domain state with high remanent magnetization was probably possible due to a high energy barrier that was required to be overcome for nucleation of local vortex in a continuous film where spins are strongly exchanged in parallel. In addition, the dipole-dipole interaction between periodically structured elements can effectively resist vortex formation which is analog to close packed magnetic dots.[19]

Now, we turn to explain the satellite feature in Fig. 2(c). The anisotropy in the films is contributed from film's induced and topographic anisotropies:

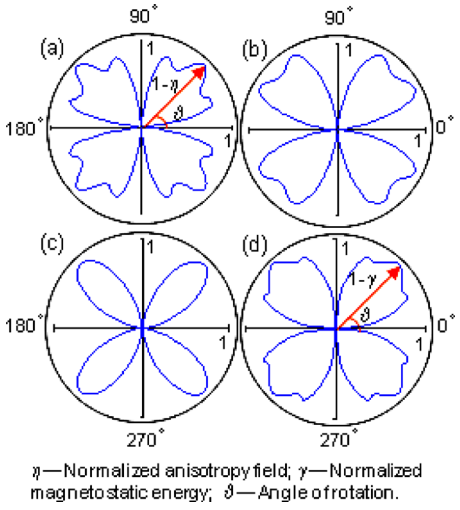

FIG. 6. (Color online) Analytical angle dependence of surface topographic anisotropy field (a)–(c) and simulated angle dependence of magnetostatic energy (d) in thin patterned films plotted in inverse polarity. (a) fourfold, eightfold, and 12-fold symmetry contributions are considered ($K_2^T=K_3^T=K_1^T/2$); (b) fourfold and eightfold symmetry terms are considered ($K_2^T=K_1^T/2$); (c) Only fourfold symmetry is considered. All curves are normalized and plotted in inverse polarity for intuitive comparison with Fig. 2(c).

$$H_K(\vartheta)=\frac{2}{\mu_0 M_S}\left[K_I\sin^2\vartheta+\sum_{\xi}K_{\xi}^T\cos^2(2\xi\vartheta)+K_0\right],$$
$$\xi=1,2,3\ldots, \tag{1}$$

where K_0 is a constant, K_I is the film's induced uniaxial anisotropy constant, and K_{ξ}^T are topographic anisotropy constants with fourfold ($\xi=1$), eightfold ($\xi=2$), 12-fold ($\xi=3$) symmetry, and so on. From a study of an isolated 2D dot array we know that higher orders of symmetry become significant when inter-dot coupling is increased.[20] In our case, the film is continuous and as such a much stronger correlation between the nanostructures is expected. Thus, an eightfold or even higher order terms of symmetry may contribute to the topographic anisotropy considerably. To confirm this we have plotted anisotropy versus angle of rotation using Eq. (1) by choosing appropriate values of K_{ξ}^T, while the film's induced anisotropy is ignored (which is a good approximation for thinner films). Figure 6(a) shows a calculated result from Eq. (1) for a normalized $H_K(\vartheta)$ curve plotted in inverse polarity. This is done for a favorable comparison with Fig. 2(c), because to a first approximation the anisotropy field is inversely proportional to remanent magnetization. In this plot, four, eight, and twelve-fold symmetry terms were included and $K_2^T=K_3^T=K_1^T/2$ has been chosen, while the $H_K(\vartheta)$ is normalized by the maximum ($H_K^{\langle 01\rangle}$) at $\langle 01\rangle$ and the minimum ($H_K^{\langle 11\rangle}$) at $\langle 11\rangle$ directions and plotted in $1-\eta$. Obviously, this curve well reproduces our experimental result in Fig. 2(c). The unevenly-weighted four branches in Fig. 2(c) [also in Figs. 3(a) and 3(c)] can be explained by a small contribution of film induced anisotropy which has some offset from the assigned original direction during plating. Figure 6 also shows topographic anisotropy curves from our analytic model when only the eightfold symmetry term is included [Fig. 6(b)] and no higher order symmetry term is considered [Fig. 6(c)]. Figure 6(d) shows a calculated angle dependence of magnetostatic energy (γ) at forced single domain state plotted with inverse polarity ($1-\gamma$). The calculation was done on a square-array-patterned (400 nm dent diameter and 400 nm separation) film with 150 nm film thickness and 100 nm surface modulation amplitude. The agreement of this calculated curve with Fig. 2(c) indicates that the anisotropic properties obtained here is the consequence of minimization of magnetostatic energy corresponding to pattern symmetry.

Although Eq. (1) is a phenomenological expression it can describe nicely the fourfold magnetic anisotropy in various cases. Apart from our results, it can also be used to fit isolated square dots, close packed dot array, single crystalline films, etc. The number of terms and amplitudes used to fit experiments contain information of film's magnetic structures and the nature of magnetic interactions between magnetic elements. For an intuitive understanding, in Fig. 5(c) we illustrate how a local magnetization is effected by its neighboring elements in our films and why higher order terms are needed for describing the anisotropy, although the real situation could be more complicated.

With increasing film thickness the angular dependence curves of coercivity experience a variation from topographic anisotropy controlled fourfold [Fig. 3(b)] to induced anisotropy controlled twofold symmetry [Fig. 3(f)]. The twofold symmetry in coercivity in Fig. 3(f) follows a near sinusoidal dependence on θ with periodicity of 180° which can be explained by magnetization rotation and domain wall propagation controlled mechanism in the magnetization reversal process. The same magnetization reversal mechanism is also expected for the fourfold coercivity governed by topographic anisotropy. One might argue that the surface modulation itself may act as "artificial roughness" to influence the measured symmetry of the coercivity's angle dependence. The coercivity caused by resistance of domain wall motion from surface roughness can be written as $H_c^r=1/2M_s(\partial\sigma_w/\partial t+\sigma_w/t)da/dx$,[21] where σ_w is the domain wall energy, t is the film thickness, and a is surface variation amplitude and da/dx is the average local surface slope induced by nanomodulation. For a film with a well defined patterned array, the domain wall will sweep over those lines which orient in the directions close to the applied magnetic field. In a square lattice the ratio of average slope "da/dx" in directions $\langle 01\rangle$, $\langle 12\rangle$, $\langle 11\rangle$ can be calculated as $da/dx\langle 01\rangle:da/dx\langle 12\rangle:da/dx\langle 11\rangle=1:2.2:1.4$, and this means that for a roughness controlled coercivity, its maximum value should not be necessarily in $\langle 11\rangle$ directions. The non-noticeable roughness effect of coercivity here can be explained by (a) the lateral dimensions of the patterned structures are much larger than the domain wall thickness and (b) the film thickness variation is small due to the conformal deposition by electroplating.

IV. CONCLUSION

We have demonstrated the ability to control anisotropy by 2D nanomodulation in continuous magnetic films. Magnetic properties, such as anisotropy field, coercivity, remanent magnetization etc. with the same symmetry as of the surface pattern has been observed. Calculation shows that the

realization of such nanomodulated films with controlled anisotropic properties is the consequence of minimization of magnetostatic energy corresponding to the pattern symmetry. To compare with other method for generating biaxial anisotropy in continuous film, such as single crystal film grown by epitaxy, the method we demonstrated here is much more flexible and low cost. For instance, anisotropy with higher symmetry (more than fourfold) can also be generated by this method and the anisotropy can be varied at different locations on a single chip simply by changing pattern geometry and layout locally.

ACKNOWLEDGMENTS

This work has been financially supported by Science Foundation Ireland Principal Investigator (SFI-PI) Grant No. 06/IN.1/I98.

[1]S. Y. Chou, Proc. IEEE **85**, 652 (1997).
[2]R. P. Cowburn, D. K. Koltsov, A. O. Adeyeye, M. E. Welland, and D. M. Tricker, Phys. Rev. Lett. **83**, 1042 (1999).
[3]S. P. Li, D. Peyrade, M. Natali, A. Lebib, Y. Chen, U. Ebels, L. D. Buda, and K. Ounadjela, Phys. Rev. Lett. **86**, 1102 (2001).
[4]C. Chappert, H. Bernas, J. Ferre, V. Kottler, J. P. Jamet, Y. Chen, E. Cambril, T. Devolder, F. Rousseaux, V. Mathet, and H. Launois, Science **280**, 1919 (1998).
[5]S. P. Li, W. S. Lew, J. A. C. Bland, L. Lopez-Diaz, M. Natali, C. A. F. Vaz, and Y. Chen, Nature **415**, 600 (2002).
[6]F. Nguyen-Van-Dau, M. Sussiau, A. Schuhl, and P. Galtier, J. Appl. Phys. **81**, 4482 (1997).
[7]D. J. Twisselmann, P. G. Chambers, C. A. Ross, G. Khanna, and B. M. Clemens, J. Appl. Phys. **92**, 3223 (2002).
[8]http://arxiv.org/ftp/arxiv/papers/0901/0901.2617.pdf
[9]W. Oepts, M. A. M. Gijs, A. Reinders, R. M. Jungblut, R. M. J. vanGansewinkel, and W. J. M. deJonge, Phys. Rev. B **53**, 14024 (1996).
[10]E. Schlömann, J. Appl. Phys. **41**, 1617 (1970).
[11]C.-H. Chang and M. H. Kryder, J. Appl. Phys. **75**, 6864 (1994).
[12]F. M. F. Rhen and S. Roy, J. Appl. Phys. **103**, 103901 (2008).
[13]S. F. Zhang and P. M. Levy, Phys. Rev. Lett. **77**, 916 (1996).
[14]G. Palasantzas, Phys. Rev. B **49**, 5785 (1994).
[15]Y. P. Zhao, H. N. Yang, G. C. Wang, and T. M. Lu, Phys. Rev. B **57**, 1922 (1998).
[16]F. Rigato, J. Geshev, V. Skumryev, and J. Fontcuberta, J. Appl. Phys. **106**, 113924 (2009).
[17]Y. P. Zhao, G. Palasantzas, G. C. Wang, and J. T. M. De Hosson, Phys. Rev. B **60**, 1216 (1999).
[18]OOMMF User's guide, National Institute of Standards and Technology, http://math.nist.gov/oommf/
[19]M. Natali, I. L. Prejbeanu, A. Lebib, L. D. Buda, K. Ounadjela, and Y. Chen, Phys. Rev. Lett. **88**, 157203 (2002).
[20]K. Y. Guslienko, Phys. Lett. A **278**, 293 (2001).
[21]Y.-P. Zhao, R. M. Gamache, G.-C. Wang, T.-M. Lu, G. Palasantzas, and J. T. M. D. Hosson, J. Appl. Phys. **89**, 1325 (2001).